Nano Energy 96 (2022) 107077

Contents lists available at ScienceDirect

Nano Energy

journal homepage: www.elsevier.com/locate/nanoen

Stretchable and transparent multimodal electronic-skin sensors in detecting strain, temperature, and humidity

Liangren Chen, Xiaohua Chang *, Han Wang, Jianwen Chen, Yutian Zhu *

College of Material, Chemistry and Chemical Engineering, Key Laboratory of Organosilicon Chemistry and Material Technology, Ministry of Education, Hangzhou Normal University, Hangzhou 311121, Zhejiang, People's Republic of China

ARTICLE INFO

Keywords:
Flexible multimodal sensor
Strain sensor
Temperature sensor
Humidity sensor
Electronic skins

ABSTRACT

Smart electronic skins (e-skins) have garnered extensive attentions owing to their potentials in health monitoring, human-machine interactions, and soft robotics. Herein, stretchable and transparent multimodal e-skin sensors composed of poly(vinyl alcohol) (PVA), citric acid (CA) and Ag nanoparticles (AgNPs) are developed by a simple *in-situ* reduction and solvent casting technology, which possess multiple sensing capabilities in strain, temperature and humidity. Although utilizing the nontransparent AgNPs as sensing components, the as-prepared PVA/CA/AgNPs sensor exhibits not only ultrahigh stretchability (up to 596% strain) but also outstanding transparency (the transmittance > 89%) attributed to the homogeneous dispersion of CA and AgNPs in PVA matrix. As flexible strain sensor, this sensor exhibits wide strain sensing range (1–200%), rapid response (90 ms), and excellent linearity of outputted signals (correlation coefficient: 0.998). Moreover, high-precision thermosensation (0.1 ℃) and outstanding temperature sensitivity (−0.076/℃ in the range of 30–40 ℃) make the sensor can detect subtle temperature variation. Furthermore, the good hygroscopicity of PVA and CA endows the fabricated sensor with outstanding humidity sensing performance, which can give human skin moisture information in real-time. More importantly, the designed sensor possesses excellent recyclability and can be reused for many times *via* the simple dissolution-reshaping treatment, which could reduce the electronical waste.

1. Introduction

Skin is the largest organ of human body, which not only protects the internal tissues and organs but also plays a critical part in our perception of the external environment [1–3]. Electronic skins (e-skins) that can imitate the features and functions of natural skin are developed to monitor various environmental stimuli, including pressure, humidity, temperature, haptics, and vibration, through real-time transforming these stimuli into the visualized electronic signals [4–6], which show great promise in intelligent robotics [7–9], human-machine interfaces [10–12], and health monitoring [13–16]. Up to now, most of e-skins are the flexible strain sensor and pressure sensor, which can only detect the strain stimulus [17–19] or the pressure stimulus [20–24]. However, human skin can sense not only the mechanical deformation but also the other environmental stimuli such as temperature and humidity [25–27]. As one of the vital functions of e-skins, temperature sensing capability can provide early warning to avoid the risk of damage from high temperature. On the other hand, the humidity monitoring is also important in our daily lives, which is related to the living environment, medical facilities, and body health. To integrate these multiple sensing functions into one electrical device, the most common strategy is to assemble different functional sensors (such as strain sensor, temperature sensor, pressure sensor, and humidity sensor) together *via* the layer-by-layer technique to a multisensory system [28–31]. For example, Zhao et al. reported a hollow MXene sphere-based flexible e-skin sensor for both strain and pressure detection by multilayer structure design [30]. However, this multilayer structure not only increases the complexity of the e-skin but also weakens the strain sensing performance of the device, such as the limitation for detecting large strain, longer response and recovery time. Moreover, it is also hard to achieve a higher temperature coefficient of resistance (TCR) as a temperature sensor for most multilayer-structured multisensory due to the structural limitation [28, 29]. Therefore, it is still a great challenge to design and fabricate multimodal e-skin sensor with excellent sensing performance by a simple strategy.

Furtherly, aiming to develop smart and green e-skins, the properties of transparency and recyclability are also desired. Transparency is needed in user-interactive displays, biomedical imaging, and touch

* Corresponding authors.
E-mail addresses: changxiaohua@hznu.edu.cn (X. Chang), ytzhu@hznu.edu.cn (Y. Zhu).

https://doi.org/10.1016/j.nanoen.2022.107077
Received 6 January 2022; Received in revised form 14 February 2022; Accepted 19 February 2022
Available online 22 February 2022

screens, where it helps to transfer information visually [32–35]. However, most of skin-like sensors are nontransparent since they are normally constructed by nontransparent conductive components (*e.g.*, carbonaceous nanoparticles, liquid metal, and conducting polymers) and stretchable polymers [19,36,37]. The high filling of nontransparent conductive components and the complex geometric structures degrade the optical transparency of the e-skins. To achieve the transparency of the sensor, the transparent ionogels or hydrogels were selected to design the transparent sensors [25,38]. For instance, Dai and coworkers fabricated a transparent and wearable strain sensor utilizing the stretchable, transparent and conductive hydrogels as the sensing component [38]. However, to date, it is still a challenge to fabricate the transparent sensor by using the nontransparent conductive components such as inorganic conductive nanoparticles. In addition, most of materials are not recycled, which may cause a large amount of waste electronics and even harm the people or pollute the environment [39,40]. To alleviate the threat of "plastic pollution", the recyclability of the e-skin devices is desirable, which can significantly reduce electronic waste and potentially decrease manufacturing cost.

Herein, we develop a flexible, transparent, recyclable and multimodal skin-like sensor with strain-, temperature-, and humidity-sensing capabilities by using polyvinyl alcohol (PVA) as substrate, citric acid (CA) as reductant and reduced silver nanoparticles (AgNPs) as conductive component. CA is selected as the reducing agent to generate AgNPs, because the carboxyl and hydroxyl groups of CA can not only easily capture Ag^+ to facilitate the homogenous distribution of Ag ions in the polymer matrix, but also enable the composite to sense humidity change and detect the relative humidity (RH) of the surrounding environment. Furtherly, CA may also act as a plasticizer in the PVA matrix to reduce the interactions among the macromolecules, resulting in the increase of the elongation at break [41]. The as-prepared PVA/CA/AgNPs sensor possesses high transparency (89%), outstanding stretchability (up to 596% strain), superior thermal sensation, and excellent humidity sensing performance. The fascinating strain sensing performance, such as fast response speed, low electrical hysteresis, outstanding sensitivity and remarkable repeatability, enable the PVA/CA/AgNPs sensor to monitor various human motions, including the facial motion and body movement. Since the conductivity of the PVA/CA/AgNPs sensor changes regularly with temperature, the sensor can be designed as a temperature sensor with excellent thermal-sensation and high detection accuracy. In addition, benefiting from the hydrophilicity of PVA and CA, the PVA/CA/AgNPs sensor can be used to light up an LED lamp in moist environment and real-time monitor the moisture on human skin. Furthermore, as we expected, the PVA-based sensor exhibits good recyclability due to the renewable PVA and CA. It is noteworthy that the reshaped sensor from the recycled PVA/CA/AgNPs composite *via* the dissolution-reshaping treatment exhibits outstanding mechanical and sensing properties even after several recycles. This study provides guidance for the fabrication of flexible, transparent, recyclable, and multisensory e-skins using the environmentally friendly resources.

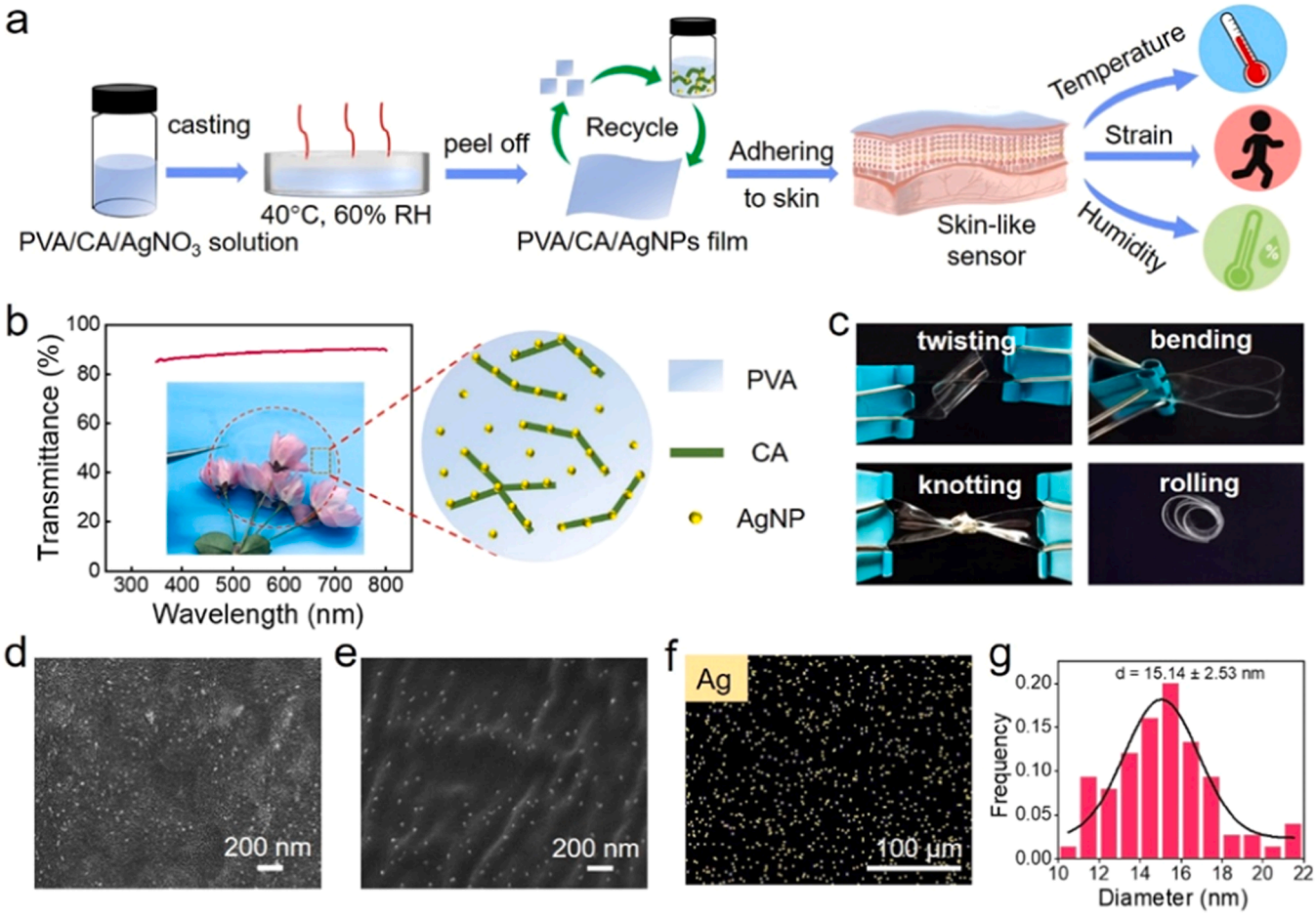

Fig. 1. Preparation and structural analysis of PVA/CA/AgNPs composite film. (a) Illustration for the fabrication of the PVA/CA/AgNPs composite film and its multisensory performance and recyclability; (b) UV–vis transmittance spectra of the film in the wavelength range from 350 to 800 nm; inset is the digital photo of the composite film. The right image is a schematic diagram showing the microstructure of PVA/CA/AgNPs composite film; (c) The optical image shows that the film is flexible enough to undergo twisting, bending, knotting, and rolling; (d) and (e) are the SEM images of the surface and the cross-section of the PVA/CA/AgNPs composite film, respectively; (f) The element (Ag) mapping on the cross section of the film; (g) The size distribution of reduced AgNPs.

2. Results and discussion

The PVA/CA/AgNPs composite films are prepared by solution casting and *in situ* reduction of $AgNO_3$ procedure, as shown in Fig. 1a. The detailed preparation of the PVA/CA/AgNPs composite films are provided in Supporting Information. The obtained composite films are denoted as PVA/CA_x/Ag_y, where x and y represent the mass ratio of CA to PVA and the mass ratio of $AgNO_3$ to PVA, respectively. The detailed compositions of different PVA/CA/AgNPs composite films are shown in Table S1. The composite films can be assembled into e-skin sensors to detect strain, temperature, and humidity stimulus. Moreover, benefiting from the water solubility and recyclability of PVA and CA, this composite film can dissolve in water and reshape again, which can still maintain multisensory abilities (Fig. 1a). The prepared PVA/CA/AgNPs composite films are highly transparent. From the photograph inserted in Fig. 1b, the picture behind the composite film can be clearly observed, indicating high transparency of the film. Quantitative investigation shows that the transmittance in the visible light range (400–800 nm) for the composite film is over 89% (Fig. 1b), which is superior to other reported e-skin materials (Table S2). This guarantees the potential application of the PVA/CA/AgNPs composite films in transparent electrode, flexible luminescent devices and other aspects, in which the transparency is essentially required. Additionally, the PVA/CA/AgNPs film can be twisted, bended, knotted and rolled, exhibiting excellent flexibility, as shown in Fig. 1c. From the scanning electron microscope (SEM) images of the PVA/CA film in Fig. S1, it is observed that both the surface and cross-section of the film are smooth and flat, indicating that the CA is well dispersed in PVA matrix. The homogeneously dispersed CA not only improves the dispersion of Ag^+ but also serves as a reducing agent for *in situ* generation of AgNPs [42,43]. Detailed reaction equation is presented in Fig. S2. In the system, to ensure the complete reduction of Ag^+ to AgNPs, CA is excessive to the amount of Ag^+. Clearly, the reduced AgNPs construct the conductive pathways in the PVA matrix, thus endowing the composites with good conductivity. To confirm the formation of AgNPs in the film, energy dispersive X-ray (EDX), SEM, UV–vis spectroscopy, and transmission electron microscopy (TEM) are conducted. As shown in Figs. 1d and 1e, numerous AgNPs are observed on the surface and fractured surface of PVA/CA/AgNPs composite film. AgNPs are also observed in TEM images for PVA/CA/AgNPs composites (Fig. S3). In addition, comparing with the UV–vis spectra of PVA and PVA/CA composite film, an absorption peak at 420 nm is observed for PVA/CA/AgNPs composite film and enhances with increasing the Ag^+ content (Fig. S4), owing to the strong surface plasmon resonance transition peak of AgNPs [44,45]. Additionally, from the EDX measurement, Ag element is homogeneously distributed at the cross-sectional surface of the film. These results confirm the successful synthesis of AgNPs *via* the *in-situ* reduction reaction, which are evenly distributed in the PVA matrix (Fig. 1 f). The average size of the obtained AgNPs is 15.1 nm with a normal distribution, as shown in Fig. 1 g.

The minimum and maximum strain detection limits of different PVA/CA/AgNPs sensors are compared in Table S3. The cyclic loading-unloading measurements of the sensors at the strain amplitude of their minimum or maximum strain detection limits are performed to examine their sensing stability and repeatability at the operating limits. Compared with other PVA/CA/AgNPs sensors with different contents of CA and AgNPs, the PVA/$CA_{0.4}$/$Ag_{0.08}$ sensor possesses lower strain sensing detection limit (1%) and the broadest sensing range (1–200%, Table S3, Supporting Information). Therefore, PVA/$CA_{0.4}$/$Ag_{0.08}$ sensor is chosen as a representative to further investigate the structural characteristics and multisensory performance of PVA/CA/AgNPs sensor. The mechanical performances of the PVA, PVA/$CA_{0.4}$, and PVA/$CA_{0.4}$/$Ag_{0.08}$ composite films are shown in Fig. S5. The Young's modulus and elongation at break for pure PVA film are 170.6 MPa and 410.7%, respectively. However, with the addition of CA, the Young's modulus greatly declines to 11.3 MPa while the elongation at break increases to 599%. This is ascribed to the plasticizing effect of the CA in the blend [41]. As for PVA/CA/AgNPs film, the Young's modulus is further reduced to 7.2 MPa, which may be due to the fact that the scattered distribution of AgNPs turns to be defects to weaken the modulus of composites [46]. The elongation at break exhibits a slight decline to 596%, attributing to the rigidity of AgNPs. The tensile stress-strain curve under cyclic stretching-releasing for PVA and PVA/CA/AgNPs composite film is presented in Fig. S6. The PVA/CA/AgNPs composite film demonstrates a lower hysteresis loop and a smaller residual strain compared to the pure PVA film in the first strain-stress curve. The PVA/CA/AgNPs composite film exhibits a residual strain of 0.54% in the first cycle at 10% strain (Fig. S6d). In the subsequent nine loading-unloading cycles, the composite film exhibits the same residual strain. Therefore, the PVA/CA/AgNPs composite film exhibits higher stretchability and excellent resilience after the first stress-strain cycle. Though the residual strain increases with the increase of strain (the residual strain is 5.4% at 100% strain and 30.8% at 200% strain, respectively), the stress-strain curves after the first cycle almost completely coincide, further implying the superior elasticity and resilience of the composite film compared to the neat PVA film (The residual strain is 1.4% at 10% strain, 23.1% at 100% strain, and 101.5% at 200% strain, respectively) (Fig. S6).

The conductivity of the PVA/$CA_{0.4}$/$Ag_{0.08}$ is 0.28 mS/m (T = 25 ℃, RH = 50%). The conductivity of composite film derives from the reduced AgNPs, which forms the conductive pathways. Based on the considerable mechanical properties, such as excellent stretchability and good resilience, the as-prepared PVA/CA/AgNPs composite film can be designed into resistive-type strain sensors. As depicted in Fig. 2a, the relative resistance change ($\Delta R/R_0$) of the PVA/CA/AgNPs sensor increases with increasing strain. As the sensor is stretched, the AgNPs networks are broken and the tunneling distance between the AgNPs are increased, which induces the increase of resistance. In contrast, as the sensor is released to its initial state, the conductive pathways of AgNPs are rebuilt, thus causing the decrease of resistance. That is, strain stimulus can be converted to detectable resistance variation. To further evaluate the sensitivity of the strain sensor, the variation of $\Delta R/R_0$ with strain is plotted and linearly fitted in Fig. 2a. As can be seen, the calculated gauge factor (GF $= \frac{\Delta R/R_0}{\Delta \varepsilon}$) is 1.6 and the correlation coefficient (R^2) is 0.998, exhibiting excellent linearity of sensing signals. The step-up strain sensing properties are related to the variable strain/deformation of the sensor, which is important for detecting the amplitude of the daily body movement. Fig. 2b demonstrates that as the step of strain increases from 1% to 5% at a rate of 1%, the resistance increases correspondingly, and the response of two cycles are almost consistent with each other. Similarly, reproducible and reversible response is observed as the step of strain increases from 10% to 50% at a rate of 10% (Fig. 2c). This result indicates that the sensor can detect different strain well and exhibits good sensing stability. Cyclically stretching PVA/CA/AgNPs sensor in three cycles at the fixed strains of 1, 10, 50, 100, 150, or 200% produces repeatable and strain-dependent resistance responses (Fig. 2d), indicating high sensing discernibility and good sensing stability. Moreover, it is noted that the sensor can monitor the maximum strain of 200%. Meanwhile, the response and relaxation times are important hints for strain sensors because short response and relaxation times can avoid mechanical damages [47,48]. As presented in Fig. 2e, the sensor exhibits the rapid response time (90 ms) and relaxation time (240 ms) when it is stretched to 1% at a high stretching rate of 1000 mm/min, which shows faster response compared with recently published reports (Table S2). In addition, the strain sensor exhibits stable and repeatable $\Delta R/R_0$ signals during continuous stretching-releasing for 200 cycles at 50% strain (Fig. 2 f), suggesting its good sensing durability and high sensitivity.

Attributed to the thermal response of the AgNPs toward ambient temperature, the fabricated PVA/CA/AgNPs sensor could be utilized as temperature sensor to sense the heat stimulus. The temperature-controlled hot stage is employed to examine the temperature sensing performance of PVA/CA/AgNPs sensor. Fig. 3a depicts that the sensor

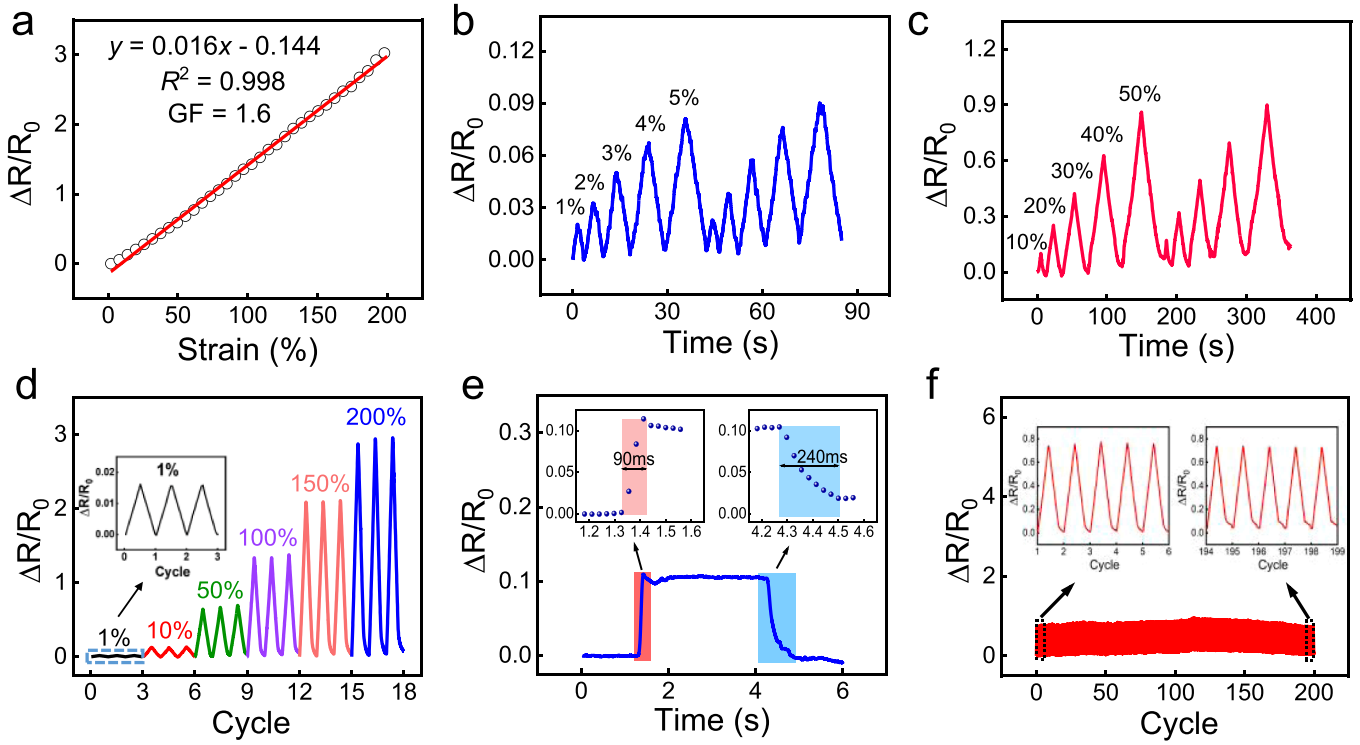

Fig. 2. Strain sensing performances of the PVA/CA/AgNPs sensor. (a) Resistance response of the sensor *versus* the applied strain from 0% to 200%. The red line represents the linear fitting curve; (b) Resistance response with stepwise increasing strain from 1% to 5% at a gradient of 1% in two cycles; (c) Resistance response from 10% to 50% with step up strain (10%) in two cycles; (d) Resistance response of the sensor under cyclic stretching-releasing deformation at various applied strains; (e) Response and relaxation time of the sensor at 1% strain with a rate of 1000 mm/min; (f) Durability and stability of PVA/CA/AgNPs strain sensor in 200 stretching-releasing cycles under 50% strain (the insets present the response signals of 1–6 and 194–199 cycles, respectively). The initial resistance, R_0 is measured at 25 ℃ and 50% RH.

exhibits a negative temperature coefficient effect and a monotonic resistance-temperature dependence from 30 to 70 ℃. The increasing electrical conductivity with temperature is because more electrons can gain energy to overcome the energy barrier at elevated temperature [46]. As seen in Fig. 3a, the resistance change rate has a nearly linear dependence on temperature in the range of 30–40 ℃, and the fitted linear equation is $y = 2.23 - 0.076x$, $R^2 = 0.972$. Interestingly, the TCR is − 0.076/℃ in the range of 30–40 ℃, which is superior to other reported e-skin temperature sensors (Table S2). In addition, as shown in Fig. 3a, the calculated TCR values are − 0.017/℃ and − 0.003/℃ in the range of 40–50 ℃ and 50–70 ℃, respectively. Fig. 3b depicts that the $\Delta R/R_0$ value of the sensor gradually decreases from 35 to 40 ℃ at a gradient of 0.5 ℃ and then maintains at a certain value as the temperature transiently stabilizes, suggesting that the sensor can accurately detect the temperature change in real time. In addition, the temperature-resistance behavior of the PVA/CA/AgNPs sensor with different heating rate is shown in Fig. 3c. To make the resistance signal keep stable before test, the temperature is held constant at 30 °C for 10 s. It is observed that the variation of $\Delta R/R_0$ is almost the same as the temperature varies from 30 to 40 ℃ under different heating rates (*e.g.*, 5, 10, 20, and 30 ℃/min), indicating that the change of resistance only depends on the amplitude of variation of temperature. Interestingly, the sensor can be capable of detecting very tiny temperature changes. As shown in Fig. S7a, the $\Delta R/R_0$ changes when the temperature ranges from 37 to 38 °C with intervals of 0.1 °C, indicating the distinguishability of the sensor is estimated to be 0.1 °C. Even at higher temperature range (65–66 ℃), the sensor can still detect a temperature change of 0.1 °C (Fig. S7b). The lower temperature monitoring accuracy demonstrates the great potential application in body temperature monitoring. The resistance responses of PVA/CA/AgNPs sensor to temperature upon exerting different strains (*e.g.*, 0%, 20%, and 50% strains) are measured in the temperature range of 30–40 ℃. Fig. 3d shows all the resistance curves are almost overlapped with increasing the temperature, indicating that the sensor is appropriate to be used as stretchable temperature sensor. Meanwhile, the strain sensing performances of the sensor under 50% strain at different temperatures (*e.g.*, 25, 35 or 50 ℃) are also tested. It is observed that the resistance curves are approximately the same (Fig. 3e), suggesting that the sensor could output stable response signals at a wide temperature range. Furthermore, the long-term stability of PVA/CA/AgNPs sensor is also studied (Fig. 3 f). After placing the sensor at 25 ℃ and 50% RH for 120 h, the resistance of the sensor remains almost unchanged, implying the sensor can be suitable for long time usage.

Furtherly, owning to the hygroscopic nature of CA and PVA, the resistance of PVA/CA/AgNPs composite film is also sensitive to humidity changes, making it potential as humidity sensors. The mechanism of PVA/CA/AgNPs humidity sensor can be explained that the CA and PVA could easily absorb moisture due to their abundant hydrophilic groups and hold it. Therefore, more conductive pathways are constructed in the film to increase the conductivity of the sensor, as illustrated in Fig. 4a. On the other hand, the absorbed moisture promotes the dissociation of CA molecule to hydrogen ions and citrate, which results in the increase of the conducting mediums [43,49,50]. The specific humidity sensing performance of PVA/CA/AgNPs sensor is shown in Figs. 4b and 4c. Fig. 4b demonstrates that $\Delta R/R_0$ decreases instantly as the RH increases from 30% to 90% at room temperature. At the same time, the humidity sensing capability of PVA/CA/AgNPs composite film is simply visualized by the brightness of a connected light-emitting diode (LED) light. A higher LED brightness is presented with increasing the RH. The moisture absorption/desorption cyclic tests in the relative humidity range of 50–90% are examined to evaluate the reliability of the humidity sensor. It is observed that the $\Delta R/R_0$ response exhibits no obvious hysteresis behavior; this indicates the sensor possesses good humidity sensing reproducibility (Fig. 4c). Based on the

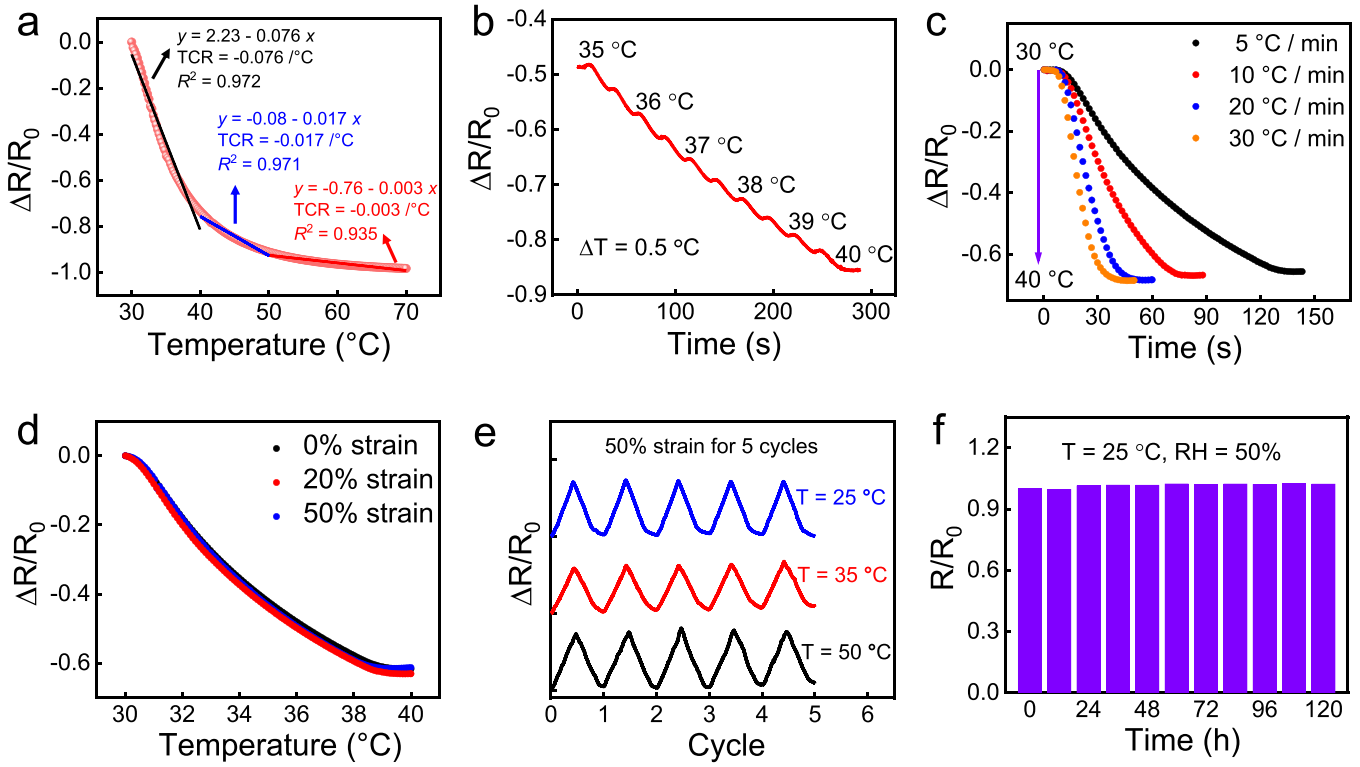

Fig. 3. Temperature sensing performances of PVA/CA/AgNPs sensor. (a) Relative resistance variation with increasing temperature from 30 to 70 ℃ (Linear fitting of the curve in the range of 30–40 ℃, 40–50 ℃, and 50–70 ℃, respectively.); (b) Relative resistance changes depending on the temperature, with increments of 0.5 ℃ from 35 to 40 ℃; (c) Comparison of the temperature-resistance response of the sensor under different heating rates in the range of 30–40 ℃; (d) Resistance response of the sensor in the range of 30–40 ℃ under different strains; (e) Resistance response of the sensor under different temperatures at a fixed strain of 50%; (f) Long-term stability of the resistance response of the sensor at the atmosphere of 25 ℃ and 50% RH.

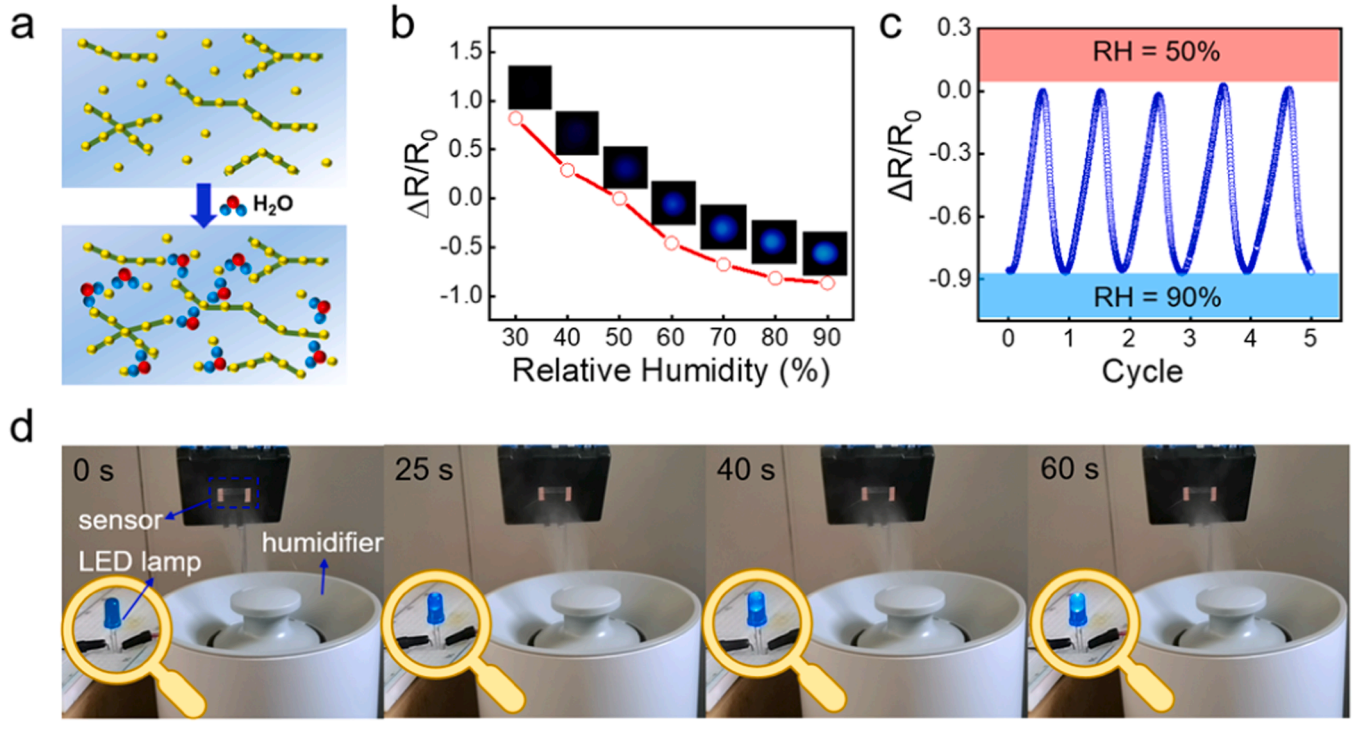

Fig. 4. Humidity sensing performances of PVA/CA/AgNPs sensor. (a) The humidity-sensing mechanism of the PVA/CA/AgNPs sensor; (b) Resistance response of the sensor and the brightness of an LED light change with RH; (c) Cyclic humidification-dehumidification response for five cycles in the humidity range of 50–90%; R_0 is measured at 25 ℃ and 50% RH; (d) The photographs of the brightness of an LED light at different times when moisture is continuously flowing on the sensor.

resistance response of the sensor to humidity, the PVA/CA/AgNPs humidity sensor can be designed to light an LED lamp. As indicated in Fig. 4d, the light is off when no moisture flow on the film. However, when exposed to moisture in a very short time (25 s), the light is on, indicating fast response to moisture. The brightness of the LED light increases with continuous humidification, making it suitable to be used as a humidity-controlled switch. The entire process is provided in Supplementary Video S1.

Supplementary material related to this article can be found online at.

In virtue of the advantages of the PVA/CA/AgNPs composite film, such as conductivity, flexibility, stretchability, thermoregulatory property, humidity sensing performance and long-term stability, the designed sensor is utilized to mimic the function of skin to response to variable stimuli. The high sensitivity and low strain detection limit of the film allow it to be employed as strain sensor for the precise recognition of real-time human subtle or large-scale movements. Fig. 5a-c record the corresponding resistance response when the sensor is integrated into the finger, wrist, and cheek under different stimuli. When the finger and wrist are bent at fixed angle, resistance response with good repeatability and stability could be produced (Figs. 5a and 5b). Tiny facial emotion such as cheek bulging can also be detected, as demonstrated in Fig. 5c. In addition, excellent thermo-sensation of well-defined PVA/CA/AgNPs temperature sensor further enables to monitor temperature change. Breathing monitoring in real time can be observed in Fig. 5d. Infrared imaging is conducted to monitor the evolution of temperature during respiration in real time. There is *ca.* 2.8 °C difference between breathing in (26.2 °C) and breathing out (29.0 °C), thus causing a significant resistance change during the respiration. Fig. 5e shows that the relative resistance decreases immediately as the sensor is approaching to a cup of hot water; however, the $\Delta R/R_0$ increases when the sensor gradually leaves the hot source and closes to a cup of cold water. Furthermore, the water content contained in skin is an essential assessment for human skin conditions, and it is an important reminder for people to use skin care products when human skin lacks water. The prepared sensor is employed to monitor the water content of facial skin and a high-precision commercial water measurement instrument is used to check the actual water contents of a volunteer's facial skin. Fig. 5 f demonstrates that the $\Delta R/R_0$ decreases after washing face (5 min later) and using moisturizer (5 min later), which is consistent well with the result of the variation of the water content of the volunteer's facial skin under different conditions.

Developing reusable sensors can greatly reduce electronic waste from a perspective of green electronics and can also potentially decrease manufacturing cost. A rectangular composite film with size of 3 cm × 1 cm can completely dissolve in water within 40 min (Fig. 6a and Supplementary Video S2). Because of the good water solubility of PVA and CA, the PVA/CA/AgNPs sensor have excellent recyclability. As shown in Fig. 6b, fractured composite films are re-dissolved to form homogeneous suspension and then reshaped with similar procedures to that used for preparing original composite films. The recycled composite films are assembled into sensors and still have excellent sensing ability to external stimuli (Fig. 6c-e). As observed in Fig. 6c, the strain sensing performances of the recycled sensor are comparable to that of original ones. It is noted that stable resistance response could be obtained for the sensor even after five runs of dissolution-remolding. In addition, when a wetting paper as a humidity source is approaching to the sensor with different height, the $\Delta R/R_0$ for the original and reshaped sensor simultaneously decreases with lowering the height between the wetting paper and the humidity sensor (Fig. 6d), demonstrating the reconstituted sensor can also accurately capture the humidity change. Furtherly, touchless temperature sensation is also achieved for the reconstituted sensor. To avoid finger humidity interference, the volunteer is wearing gloves. As shown in Fig. 6e, when the finger wearing gloves is close to the sensor with a height of 0.6 cm at room temperature (25 °C), the $\Delta R/$

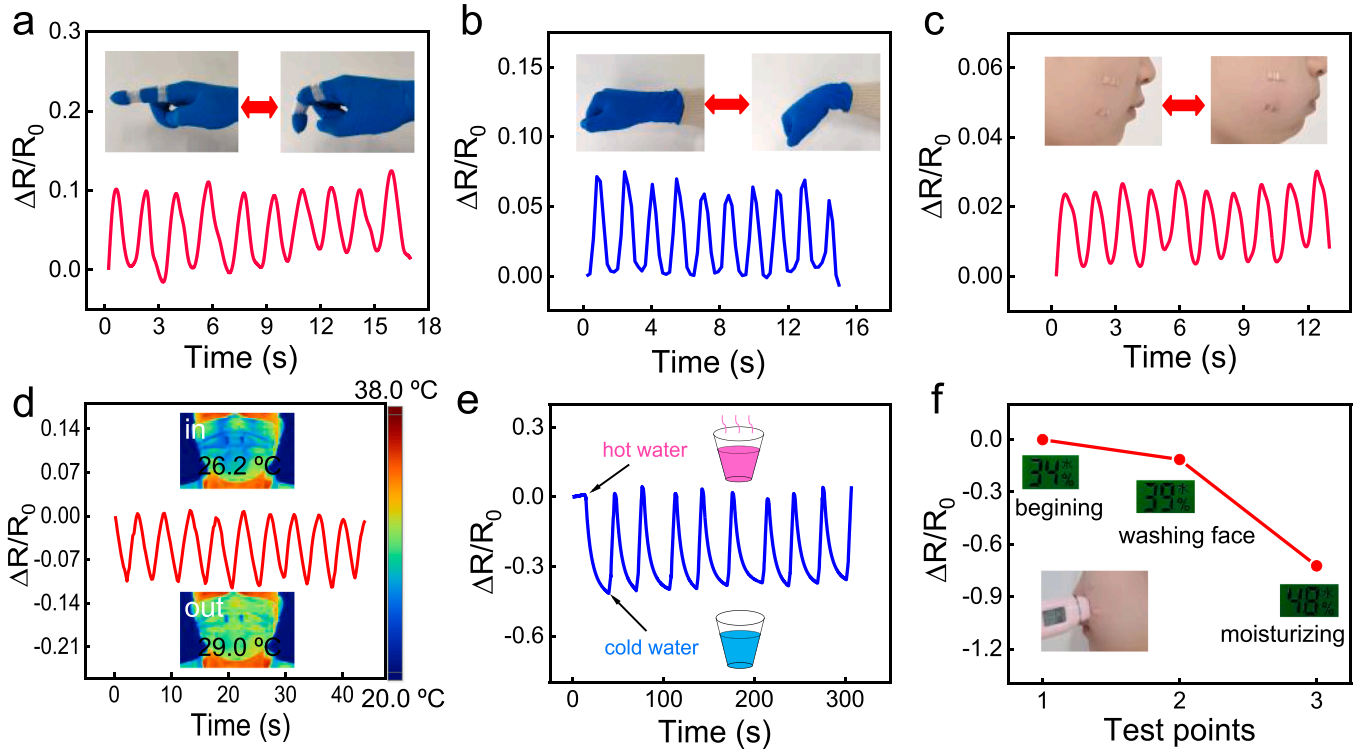

Fig. 5. Sensing applications of the PVA/CA/AgNPs-based multifunctional sensor. The strain sensor senses (a) human finger bending, (b) wrist bending, and (c) cheek bulging; (d) Resistance response to periodical exhaling; Insert is the actual temperature during respiration monitored by infrared camera; (e) Temperature-induced real-time resistance changes when the sensor is closing to a bottle of hot or cold water; (f) Relationship between the water contents of human skin and the relative resistance; a commercial water measurement instrument is used to detect the change of the facial water content when beginning of the experiment, washing the face or moisturizing.

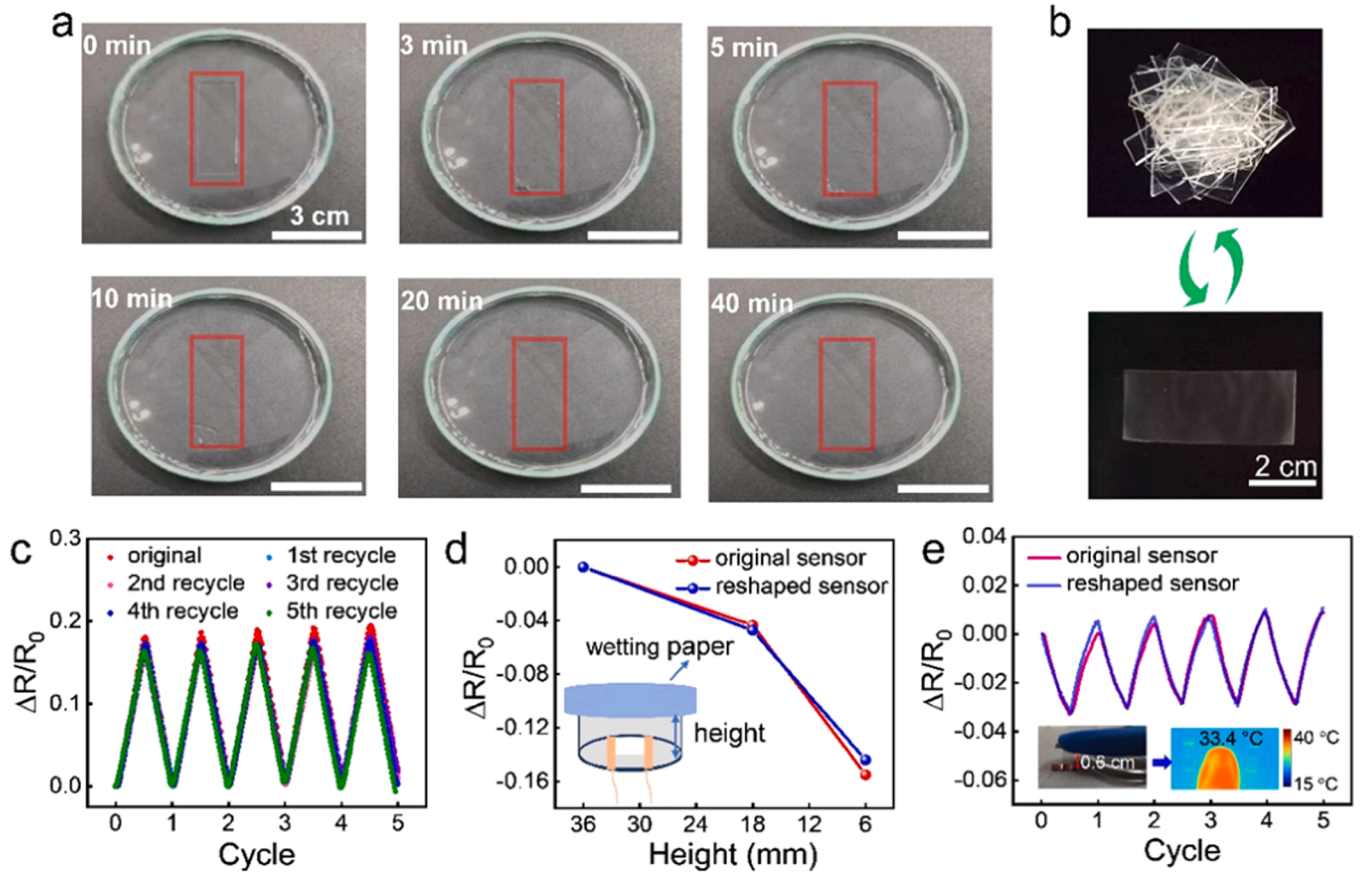

Fig. 6. (a) Illustration for the dissolution process of the composite film; The scale bar is 3 cm for all the images. (b) The recyclability of the PVA/CA/AgNPs film; (c) The strain sensing performances of the original sensor and the reshaped sensor; Response of the original sensor and the reshaped sensor (d) when the wetting paper is closing to the sensor with different height and (e) when the finger wearing gloves is approaching to the sensor.

R_0 instantly decreases. In this process, the volunteer's finger temperature is ~33.4 ℃ from the infrared camera. Thereafter, as the hot source moves away, the $\Delta R/R_0$ recovers to its original value. Resistance response for reshaped sensor is nearly identical to that of the corresponding original sensor. The above results clearly manifest that the PVA/CA/AgNPs sensor can be thought as green electronic device, which gives a great possibility to reduce the waste electronics.

Supplementary material related to this article can be found online at.

3. Conclusions

In summary, flexible, transparent, recyclable, and multimodal skin-like sensor composed of biodegradable PVA, CA and conductive AgNPs was successfully fabricated by *in-situ* reduction and solvent casting method. To the best of our knowledge, this is the first report that achieves both high stretchability (up to 596% strain) and excellent transparency (transmittance > 89%) by using the conductive polymer composites containing with the nontransparent conductive nanoparticles to fabricate the flexible sensor. As stretchable strain sensor, the designed PVA/CA/AgNPs sensors possess various merits, such as wide sensing range (1–200%), fast response (90 ms), and outstanding linearity of outputted signals (correlation coefficient: 0.998). Moreover, owing to the high temperature sensitivity of AgNPs, the sensor exhibits superior temperature sensing capability with high detection precision (0.1 ℃), high TCR (—0.076/℃) in the range of 30–40 ℃, and great durability for long-term usage. Furthermore, attributed to the hygroscopicity of PVA and CA, the as-prepared sensor presents high humidity sensitivity and stability, thus enabling to be used as skin moisture detector. Impressively, the PVA/CA/AgNPs composite films are extremely biocompatible and capable of being recycled, enabling them to be friendly to human skin and the environment. Therefore, the perfect integration of these functions ensures that the PVA/CA/AgNPs sensors have potential applications in human motion detecting, temperature and humidity monitoring, personal healthcare and thermal management. This work may inspire more researchers to explore high-performance skin-like sensors for next-generation green wearable electronics and soft robotics.

CRediT authorship contribution statement

Liangren chen: Investigation, Data curation, Methodology, Writing – original draft. **Xiaohua Chang:** Supervision, Conceptualization, Methodology, Formal analysis, Writing – review & editing. **Han Wang:** Methodology, Formal analysis. **Jianwen Chen:** Methodology, Formal analysis. **Yutian Zhu:** Supervision, Conceptualization, Methodology, Writing – review & editing.

Declaration of Competing Interest

The authors declare that they have no known competing financial interests or personal relationships that could have appeared to influence the work reported in this paper.

Acknowledgments

This work is supported by Zhejiang Provincial Natural Science Fund (LR20E030003) and National Natural Science Foundation of China (52003070).

Appendix A. Supporting information

Supplementary data associated with this article can be found in the online version at doi:10.1016/j.nanoen.2022.107077.

References

[1] S. Wang, J. Xu, W. Wang, G.N. Wang, R. Rastak, F. Molina-Lopez, J.W. Chung, S. Niu, V.R. Feig, J. Lopez, T. Lei, S.K. Kwon, Y. Kim, A.M. Foudeh, A. Ehrlich, A. Gasperini, Y. Yun, B. Murmann, J.B. Tok, Z. Bao, Skin electronics from scalable fabrication of an intrinsically stretchable transistor array, Nature 555 (2018) 83–88, https://doi.org/10.1038/nature25494.

[2] Z. Zou, C. Zhu, Y. Li, X. Lei, W. Zhang, J. Xiao, Rehealable, fully recyclable, and malleable electronic skin enabled by dynamic covalent thermoset nanocomposite, Sci. Adv. 4 (2018) eaaq0508, https://doi.org/10.1126/sciadv.aaq0508.

[3] X. Peng, K. Dong, C. Ye, Y. Jiang, S. Zhai, R. Cheng, D. Liu, X. Gao, J. Wang, Z. L. Wang, A breathable, biodegradable, antibacterial, and self-powered electronic skin based on all-nanofiber triboelectric nanogenerators, Sci. Adv. 6 (2020) eaba9624, https://doi.org/10.1126/sciadv.aba9624.

[4] K. Suzuki, K. Yataka, Y. Okumiya, S. Sakakibara, K. Sako, H. Mimura, Y. Inoue, Rapid-response, widely stretchable sensor of aligned MWCNT/elastomer composites for human motion detection, ACS Sens. 1 (2016) 817–825, https://doi.org/10.1021/acssensors.6b00145.

[5] H. Wei, D. Kong, T. Li, Q. Xue, S. Wang, D. Cui, Y. Huang, L. Wang, S. Hu, T. Wan, G. Yang, Solution-processable conductive composite hydrogels with multiple synergetic networks toward wearable pressure/strain sensors, ACS Sens. 6 (2021) 2938–2951, https://doi.org/10.1021/acssensors.1c00699.

[6] Y. Cheng, D. Wu, S. Hao, Y. Jie, X. Cao, N. Wang, Z.L. Wang, Highly stretchable triboelectric tactile sensor for electronic skin, Nano Energy 64 (2019), 103907, https://doi.org/10.1016/j.nanoen.2019.103907.

[7] G. Jin, Y. Sun, J. Geng, X. Yuan, T. Chen, H. Liu, F. Wang, L. Sun, Bioinspired soft caterpillar robot with ultra-stretchable bionic sensors based on functional liquid metal, Nano Energy 84 (2021), 105896, https://doi.org/10.1016/j.nanoen.2021.105896.

[8] J. Chen, Y. Zhu, Z. Guo, A.G. Nasibulin, Recent progress on thermo-electrical properties of conductive polymer composites and their application in temperature sensors, Eng. Sci. 12 (2020) 13–22, https://doi.org/10.30919/es8d1129.

[9] L. Shuai, Z.H. Guo, P. Zhang, J. Wan, X. Pu, Z.L. Wang, Stretchable, self-healing, conductive hydrogel fibers for strain sensing and triboelectric energy-harvesting smart textiles, Nano Energy 78 (2020), 105389, https://doi.org/10.1016/j.nanoen.2020.105389.

[10] M. Li, J. Chen, W. Zhong, M. Luo, W. Wang, X. Qing, Y. Lu, Q. Liu, K. Liu, Y. Wang, D. Wang, Large-area, wearable, self-powered pressure-temperature sensor based on 3D thermoelectric spacer fabric, ACS Sens. 5 (2020) 2545–2554, https://doi.org/10.1021/acssensors.0c00870.

[11] F. Xu, S. Dong, G. Liu, C. Pan, Z.H. Guo, W. Guo, L. Li, Y. Liu, C. Zhang, X. Pu, Z. L. Wang, Scalable fabrication of stretchable and washable textile triboelectric nanogenerators as constant power sources for wearable electronics, Nano Energy 88 (2021), 106247, https://doi.org/10.1016/j.nanoen.2021.106247.

[12] C. Hang, X. Zhao, S. Xi, Y. Shang, K. Yuan, F. Yang, Q. Wang, J. Wang, D.W. Zhang, H. Lu, Highly stretchable and self-healing strain sensors for motion detection in wireless human-machine interface, Nano Energy 76 (2020), 105064, https://doi.org/10.1016/j.nanoen.2020.105064.

[13] T. Yang, X. Jiang, Y. Zhong, X. Zhao, S. Lin, J. Li, X. Li, J. Xu, Z. Li, H. Zhu, A wearable and highly sensitive graphene strain sensor for precise home-based pulse wave monitoring, ACS Sens. 2 (2017) 967–974, https://doi.org/10.1021/acssensors.7b00230.

[14] K.-Y. Chun, S. Seo, C.-S. Han, Self-powered, stretchable, and wearable ion gel mechanoreceptor sensors, ACS Sens. 6 (2021) 1940–1948, https://doi.org/10.1021/acssensors.1c00346.

[15] J.-H. Pu, X. Zhao, X.-J. Zha, W.-D. Li, K. Ke, R.-Y. Bao, Z.-Y. Liu, M.-B. Yang, W. Yang, A strain localization directed crack control strategy for designing MXene-based customizable sensitivity and sensing range strain sensors for full-range human motion monitoring, Nano Energy 74 (2020), 104814, https://doi.org/10.1016/j.nanoen.2020.104814.

[16] M. Chao, Y. Wang, D. Ma, X. Wu, W. Zhang, L. Zhang, P. Wan, Wearable MXene nanocomposites-based strain sensor with tile-like stacked hierarchical microstructure for broad-range ultrasensitive sensing, Nano Energy 78 (2020), 105187, https://doi.org/10.1016/j.nanoen.2020.105187.

[17] J. Mao, C. Zhao, L. Liu, Y. Li, D. Xiang, Y. Wu, H. Li, Adhesive, transparent, stretchable, and strain-sensitive hydrogel as flexible strain sensor, Compos. Commun. 25 (2021), 100733, https://doi.org/10.1016/j.coco.2021.100733.

[18] J. Zeng, W. Ma, Q. Wang, S. Yu, M.T. Innocent, H. Xiang, M. Zhu, Strong, high stretchable and ultrasensitive SEBS/CNTs hybrid fiber for high-performance strain sensor, Compos. Commun. 25 (2021), 100735, https://doi.org/10.1016/j.coco.2021.100735.

[19] J. Chen, Y. Zhu, W. Jiang, A stretchable and transparent strain sensor based on sandwich-like PDMS/CNTs/PDMS composite containing an ultrathin conductive CNT layer, Compos. Sci. Technol. 186 (2020), 107938, https://doi.org/10.1016/j.compscitech.2019.107938.

[20] Y.C. Lai, J. Deng, R. Liu, Y.C. Hsiao, S.L. Zhang, W. Peng, H.M. Wu, X. Wang, Z. L. Wang, Actively perceiving and responsive soft robots enabled by self-powered, highly extensible, and highly sensitive triboelectric proximity- and pressure-sensing skins, Adv. Mater. 30 (2018) 1801114, https://doi.org/10.1002/adma.201801114.

[21] G. Yao, L. Xu, X. Cheng, Y. Li, X. Huang, W. Guo, S. Liu, Z.L. Wang, H. Wu, Bioinspired triboelectric nanogenerators as self-powered electronic skin for robotic tactile sensing, Adv. Funct. Mater. 30 (2020) 1907312, https://doi.org/10.1002/adfm.201907312.

[22] X. Wang, H. Zhang, L. Dong, X. Han, W. Du, J. Zhai, C. Pan, Z.L. Wang, Self-powered high-resolution and pressure-sensitive triboelectric sensor matrix for real-time tactile mapping, Adv. Mater. 28 (2016) 2896–2903, https://doi.org/10.1002/adma.201503407.

[23] Z. Ren, J. Nie, J. Shao, Q. Lai, L. Wang, J. Chen, X. Chen, Z.L. Wang, Fully elastic and metal-free tactile sensors for detecting both normal and tangential forces based on triboelectric nanogenerators, Adv. Funct. Mater. 28 (2018) 1802989, https://doi.org/10.1002/adfm.201802989.

[24] C. Zhang, S. Liu, X. Huang, W. Guo, Y. Li, H. Wu, A stretchable dual-mode sensor array for multifunctional robotic electronic skin, Nano Energy 62 (2019) 164–170, https://doi.org/10.1016/j.nanoen.2019.05.046.

[25] N. Jiang, X. Chang, D. Hu, L. Chen, Y. Wang, J. Chen, Y. Zhu, Flexible, transparent, and antibacterial ionogels toward highly sensitive strain and temperature sensors, Chem. Eng. J. 424 (2021), 130418, https://doi.org/10.1016/j.cej.2021.130418.

[26] J. Sun, R. Li, G. Lu, Y. Yuan, X. Zhu, J. Nie, A facile strategy for fabricating multifunctional ionogel based electronic skin, J. Mater. Chem. C. 8 (2020) 8368–8373, https://doi.org/10.1039/d0tc01057j.

[27] X. Guan, Z. Hou, K. Wu, H. Zhao, S. Liu, T. Fei, T. Zhang, Flexible humidity sensor based on modified cellulose paper, Sens. Actuators B Chem. 339 (2021), 129879, https://doi.org/10.1016/j.snb.2021.129879.

[28] M. Han, L. Chen, K. Aras, C. Liang, X. Chen, H. Zhao, K. Li, N.R. Faye, B. Sun, J. H. Kim, W. Bai, Q. Yang, Y. Ma, W. Lu, E. Song, J.M. Baek, Y. Lee, C. Liu, J. B. Model, G. Yang, R. Ghaffari, Y. Huang, I.R. Efimov, J.A. Rogers, Catheter-integrated soft multilayer electronic arrays for multiplexed sensing and actuation during cardiac surgery, Nat. Biomed. Eng. 4 (2020) 997–1009, https://doi.org/10.1038/s41551-020-00604-w.

[29] Q. Hua, J. Sun, H. Liu, R. Bao, R. Yu, J. Zhai, C. Pan, Z.L. Wang, Skin-inspired highly stretchable and conformable matrix networks for multifunctional sensing, Nat. Commun. 9 (2018) 244, https://doi.org/10.1038/s41467-017-02685-9.

[30] X.F. Zhao, X.H. Wen, S.L. Zhong, M.Y. Liu, Y.H. Liu, X.B. Yu, R.G. Ma, D.W. Zhang, J.C. Wang, H.L. Lu, Hollow MXene sphere-based flexible e-skin for multiplex tactile detection, ACS Appl. Mater. Interfaces 13 (2021) 45924–45934, https://doi.org/10.1021/acsami.1c06993.

[31] K. Xu, Y. Lu, T. Yamaguchi, T. Arie, S. Akita, K. Takei, Highly precise multifunctional thermal management-based flexible sensing sheets, ACS Nano 13 (2019) 14348–14356, https://doi.org/10.1021/acsnano.9b07805.

[32] X. Wang, Y. Zhang, X. Zhang, Z. Huo, X. Li, M. Que, Z. Peng, H. Wang, C. Pan, A highly stretchable transparent self-powered triboelectric tactile sensor with metallized nanofibers for wearable electronics, Adv. Mater. 30 (2018) 1706738, https://doi.org/10.1002/adma.201706738.

[33] Q. Wang, M. Jian, C. Wang, Y. Zhang, Carbonized silk nanofiber membrane for transparent and sensitive electronic skin, Adv. Funct. Mater. 27 (2017) 1605657, https://doi.org/10.1002/adfm.201605657.

[34] X. Chang, L. Chen, J. Chen, Y. Zhu, Z. Guo, Advances in transparent and stretchable strain sensors, Adv. Compos. Hybrid Mater. 4 (2021) 435–450, https://doi.org/10.1007/s42114-021-00292-3.

[35] N. Jiang, D. Hu, Y. Xu, J. Chen, X. Chang, Y. Zhu, Y. Li, Z. Guo, Ionic liquid enabled flexible transparent polydimethylsiloxane sensors for both strain and temperature sensing, Adv. Compos. Hybrid Mater. 4 (2021) 574–583, https://doi.org/10.1007/s42114-021-00262-9.

[36] H. Liao, X. Guo, P. Wan, G. Yu, Conductive MXene nanocomposite organohydrogel for flexible, healable, low-temperature tolerant strain sensors, Adv. Funct. Mater. 29 (2019) 1904507, https://doi.org/10.1002/adfm.201904507.

[37] H. Li, J. Chen, X. Chang, Y. Xu, G. Zhao, Y. Zhu, Y. Li, A highly stretchable strain sensor with both an ultralow detection limit and an ultrawide sensing range, J. Mater. Chem. A 9 (2021) 1795–1802, https://doi.org/10.1039/d0ta10990h.

[38] H. Sun, Y. Zhao, C. Wang, K. Zhou, C. Yan, G. Zheng, J. Huang, K. Dai, C. Liu, C. Shen, Ultra-stretchable, durable and conductive hydrogel with hybrid double network as high performance strain sensor and stretchable triboelectric nanogenerator, Nano Energy 76 (2020), 105035, https://doi.org/10.1016/j.nanoen.2020.105035.

[39] R. Pan, W. Xuan, J. Chen, S. Dong, H. Jin, X. Wang, H. Li, J. Luo, Fully biodegradable triboelectric nanogenerators based on electrospun polylactic acid and nanostructured gelatin films, Nano Energy 45 (2018) 193–202, https://doi.org/10.1016/j.nanoen.2017.12.048.

[40] S. Wang, J.Y. Oh, J. Xu, H. Tran, Z. Bao, Skin-inspired electronics: an emerging paradigm, Acc. Chem. Res. 51 (2018) 1033–1045, https://doi.org/10.1021/acs.accounts.8b00015.

[41] R. Shi, J. Bi, Z. Zhang, A. Zhu, D. Chen, X. Zhou, L. Zhang, W. Tian, The effect of citric acid on the structural properties and cytotoxicity of the polyvinyl alcohol/starch films when molding at high temperature, Carbohydr. Polym. 74 (2008) 763–770, https://doi.org/10.1016/j.carbpol.2008.04.045.

[42] P. Filipczak, M. Borkowski, P. Chudobinski, S. Bres, M. Matusiak, G. Nowaczyk, M. Kozanecki, Sodium citrate stabilized Ag NPs under thermal treatment, electron-beam and laser irradiations, Radiat. Phys. Chem. 169 (2020), 107948, https://doi.org/10.1016/j.radphyschem.2018.07.020.

[43] C. Xu, Z. Zheng, M. Lin, Q. Shen, X. Wang, B. Lin, L. Fu, Strengthened, antibacterial, and conductive flexible film for humidity and strain sensors, ACS Appl. Mater. Interfaces 12 (2020) 35482–35492, https://doi.org/10.1021/acsami.0c10101.

[44] M.E. El-Naggar, T.I. Shaheen, M.M. Fouda, A.A. Hebeish, Eco-friendly microwave-assisted green and rapid synthesis of well-stabilized gold and core-shell silver-gold nanoparticles, Carbohydr. Polym. 136 (2016) 1128–1136, https://doi.org/10.1016/j.carbpol.2015.10.003.
[45] S. Hao, C. Shao, L. Meng, C. Cui, F. Xu, J. Yang, Tannic acid-silver dual catalysis induced rapid polymerization of conductive hydrogel sensors with excellent stretchability, self-adhesion, and strain-sensitivity properties, ACS Appl. Mater. Interfaces 12 (2020) 56509–56521, https://doi.org/10.1021/acsami.0c18250.
[46] R. Yin, S. Yang, Q. Li, S. Zhang, H. Liu, J. Han, C. Liu, C. Shen, Flexible conductive Ag nanowire/cellulose nanofibril hybrid nanopaper for strain and temperature sensing applications, Sci. Bull. 65 (2020) 899–908, https://doi.org/10.1016/j.scib.2020.02.020.
[47] Y. Zhou, P. Zhan, M. Ren, G. Zheng, K. Dai, L. Mi, C. Liu, C. Shen, Significant stretchability enhancement of a crack-based strain sensor combined with high sensitivity and superior durability for motion monitoring, ACS Appl. Mater. Interfaces 11 (2019) 7405–7414, https://doi.org/10.1021/acsami.8b20768.
[48] Y. Yu, G. Zheng, K. Dai, W. Zhai, K. Zhou, Y. Jia, G. Zheng, Z. Zhang, C. Liu, C. Shen, Hollow-porous fibers for intrinsically thermally insulating textiles and wearable electronics with ultrahigh working sensitivity, Mater. Horiz. 8 (2021) 1037–1046, https://doi.org/10.1039/D0MH01818J.
[49] Y. Chen, J. Nie, C. Xu, W. Wu, Z. Zheng, Strengthened, recyclable, weldable, and conducting-controllable biobased rubber film with a continuous water-soluble framework network, ACS Sustain, Chem. Eng. 8 (2020) 1285–1294, https://doi.org/10.1021/acssuschemeng.9b06644.
[50] T. Li, L. Li, H. Sun, Y. Xu, X. Wang, H. Luo, Z. Liu, T. Zhang, Porous ionic membrane based flexible humidity sensor and its multifunctional applications, Adv. Sci. 4 (2017) 1600404, https://doi.org/10.1002/advs.201600404.

Liangren Chen obtained her bachelor degree from Hangzhou Normal University in 2020. Now she is a graduate student in College of Material, Chemistry and Chemical Engineering, Key Laboratory of Organosilicon Chemistry and Material Technology, Ministry of Education at Hangzhou Normal University. Her research interests mainly focus on the design and applications of conductive polymer composites-based sensors.

Xiaohua Chang received her Bachelor Degree in 2014 from Hefei University of Technology and her Ph.D. in Chemical Engineering and Technology from Zhejiang University in 2019 under the supervision of Prof. Pengju Pan. Currently, she is a lecturer in College of Material, Chemistry and Chemical Engineering, Key Laboratory of Organosilicon Chemistry and Material Technology, Ministry of Education, Hangzhou Normal University. Her present research efforts concentrate on the self-assembly of stimuli-responsive polymer and stretchable sensors based on conductive polymer nanocomposites.

Han Wang obtained his bachelor degree from Chizhou University in 2021. Now he is a graduate student in College of Material, Chemistry and Chemical Engineering, Key Laboratory of Organosilicon Chemistry and Material Technology, Ministry of Education at Hangzhou Normal University. He is now working on the design and application of ionogel-based flexible multifunctional sensors.

Jianwen Chen received her Ph.D. in State Key Laboratory of Polymer Physics and Chemistry, Changchun Institute of Applied Chemistry, Chinese Academy of Sciences. Currently, she is a lecturer in College of Material, Chemistry and Chemical Engineering, Key Laboratory of Organosilicon Chemistry and Material Technology, Ministry of Education, Hangzhou Normal University. Her research interests focus on multifunctional polymer-based nanocomposites, especially conductive polymer composite based sensors.

Yutian Zhu obtained his Ph.D. in Polymer Chemistry and Physics from Changchun Institute of Applied Chemistry, Chinese Academy of Sciences in 2006. Then, he achieved his 4-year postdoctoral training in KU Leuven and University of Memphis, respectively. In 2010, he became an associate professor in State Key Laboratory of Polymer Physics and Chemistry at Changchun Institute of Applied Chemistry, Chinese Academy of Sciences. Then, he served as a full professor at the College of Material, Chemistry and Chemical Engineering, Hangzhou Normal University since 2018. His current research focuses on the multicomponent polymer nanocomposites and their applications in flexible sensors.